Damage prediction in Incremental Forming

Thesis committee presentation

Carlos Felipe Guzmán

MS^{2}F Sector
Department ArGEnCo
University of Liège, Belgium
cf.guzman@ulg.ac.be

August 28th, 2013

Contents

Contents

Single point incremental forming

- A sheet metal is deformed by a small tool.
- The tool could be guided by a CNC (milling machine, robot).

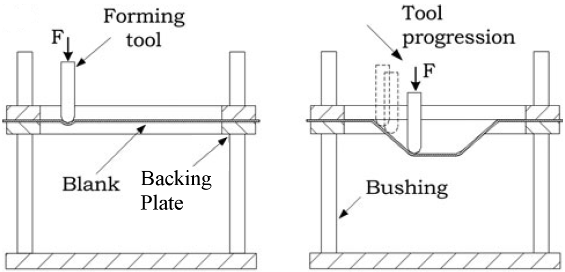

[Henrard et al., 2010]

Single point incremental forming

- **Dieless**, with high sheet formability.
- Easy shape generation.
- For rapid prototypes, small batch productions, etc.

Single point incremental forming

- **Dieless**, with high sheet formability.
- Easy shape generation.
- For rapid prototypes, small batch productions, etc.

Challenges

- Geometrical inaccuracy.
- Process mechanics.
- Increased formability.

Single point incremental forming

- **Dieless**, with high sheet formability.
- Easy shape generation.
- For rapid prototypes, small batch productions, etc.

Challenges

- Geometrical inaccuracy.
- Process mechanics.
- Increased formability.

Motivations

- Through the thickness gradient are important.
- 2D constitutive laws cannot be used.
- New advances on element formulation in FE codes.

Goals and cooperations

- Improve the FEM simulations for SPIF.
  - Solid Shell element (A. Ben Bettaieb thesis, ULg).
  - Remeshing method (J. Sena thesis, UAveiro, Portugal).
  - Validations (Joost Duflou team, KULeuven).

Goals and cooperations

- Improve the FEM simulations for SPIF.
  - Solid Shell element (A. Ben Bettaieb thesis, ULg).
  - Remeshing method (J. Sena thesis, UAveiro, Portugal).
  - Validations (Joost Duflou team, KULeuven).
- Understand the rupture mechanism during SPIF process.
  - Metallurgical study, porosity and texture (A. Mertens, ULg).
  - Extended Gurson model.

Goals and cooperations

- Improve the FEM simulations for SPIF.
  - Solid Shell element (A. Ben Bettaieb thesis, ULg).
  - Remeshing method (J. Sena thesis, UAveiro, Portugal).
  - Validations (Joost Duflou team, KULeuven).
- Understand the rupture mechanism during SPIF process.
  - Metallurgical study, porosity and texture (A. Mertens, ULg).
  - Extended Gurson model.
- Reach a better understanding of the process.
  - Deformation mechanisms (A. Kumar Behera thesis, KULeuven).
  - Formability analysis.
  - Texture evolution and damage.

Contents

SPIF simulations

- **FE code**: LAGAMINE (implicit).
- **Element type**: COQJ4 (shell) and SSH3D (solid-shell).
- **Sheet material**: AA3003-O and DC01 steel (new).

SPIF simulations

- **FE code**: LAGAMINE (implicit).
- **Element type**: COQJ4 (shell) and SSH3D (solid-shell).
- **Sheet material**: AA3003-O and DC01 steel (new).
- **Tests**:

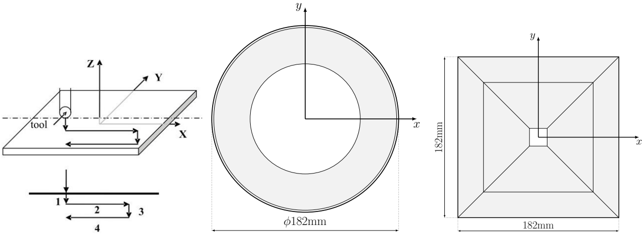

(a) Line test (b) Cone (c) Pyramid

Simulations

- Material: DC01 ferritic steel (1 mm thickness).
- Two slope pyramid:

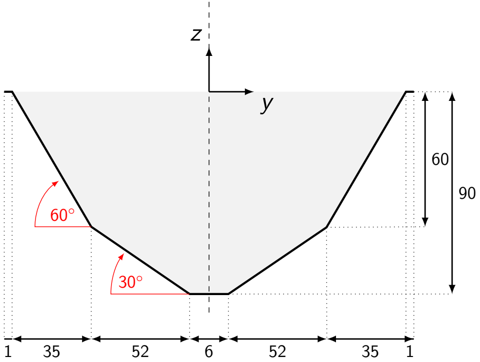

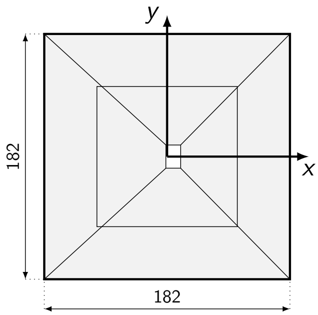

Constitutive modeling

- Isotropic elasto-plastic constitutive law.
- Voce (isotropic) and Armstrong-Frederick (kinematic) mixed hardening.

$$\sigma_Y = \sigma_{Y0} + K\left(1 - \exp\left(-n\epsilon^P\right)\right)$$

$$\dot{\mathbf{X}} = C_x\left(X_{sat}\dot{\boldsymbol{\epsilon}^P} - \dot{\epsilon^P}\mathbf{X}\right)$$

Constitutive modeling

- Isotropic elasto-plastic constitutive law.
- Voce (isotropic) and Armstrong-Frederick (kinematic) mixed hardening.

$$\sigma_Y = \sigma_{Y0} + K\left(1 - \exp\left(-n\epsilon^P\right)\right)$$

$$\dot{\mathbf{X}} = C_x\left(X_{sat}\dot{\boldsymbol{\epsilon}^P} - \dot{\epsilon^P}\mathbf{X}\right)$$

- Material parameters:

$$\begin{array}{lclclcl} \sigma_{Y0} & = & 158\,\text{MPa} & C_x & = & 257 \\ K & = & 255\,\text{MPa} & X_{sat} & = & 4\,\text{MPa} \\ n & = & 13 & & & \end{array}$$

- Identification through *classical* (tensile, monotonic/Bauschinger shear) tests.

Solid-shell element

SSH3D

- Enhanced assumed strain (EAS).
- Assumed natural strain (ANS).
- In-plane full integration and 5 IP through-the-thickness.

Shell element ⟷ 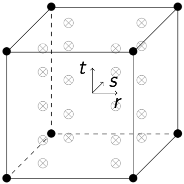 ⟷ *Brick element*

Solid-shell

Assumed natural strain

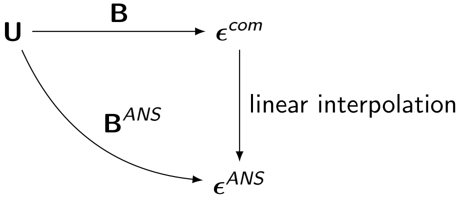

Assumed natural strain

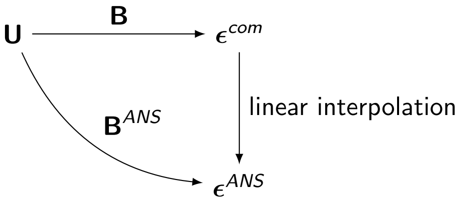

Sampling points (transverse shear and transverse normal strains):

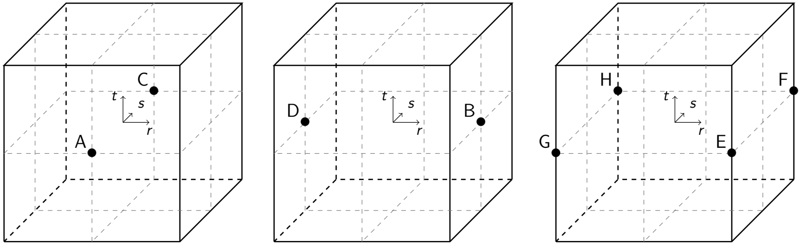

Enhanced assumed strain

Enhanced strain field

$$\boldsymbol{\epsilon} = \boldsymbol{\epsilon}^{com} + \boldsymbol{\epsilon}^{EAS}$$

$$\boldsymbol{\epsilon}^{com} = \Delta^{s}\mathbf{u} = \mathbf{B}(r, s, t)\mathbf{U}$$

$$\boldsymbol{\epsilon}^{EAS} = \mathbf{G}(r, s, t)\boldsymbol{\alpha} = \frac{|\mathrm{J}_0|}{|J(r, s, t)|}\mathbf{F}_0^{-T}\mathbf{M}(r, s, t)\boldsymbol{\alpha}$$

Enhanced assumed strain

Enhanced strain field

$$\boldsymbol{\epsilon} = \boldsymbol{\epsilon}^{com} + \boldsymbol{\epsilon}^{EAS}$$

$$\boldsymbol{\epsilon}^{com} = \Delta^{s}\mathbf{u} = \mathbf{B}(r,s,t)\mathbf{U}$$

$$\boldsymbol{\epsilon}^{EAS} = \mathbf{G}(r,s,t)\boldsymbol{\alpha} = \frac{|\mathrm{J}_0|}{|J(r,s,t)|}\mathbf{F}_0^{-T}\mathbf{M}(r,s,t)\boldsymbol{\alpha}$$

$$[\mathbf{M}] =$$

$$\begin{bmatrix}
r & 0 & 0 & 0 & 0 & 0 & 0 & 0 & 0 & 0 & 0 & 0 & 0 & 0 & 0 & rs & rt & 0 & 0 & 0 & 0 & 0 & 0 & 0 & rst & 0 & 0 & 0 & 0 & 0 \\
0 & s & 0 & 0 & 0 & 0 & 0 & 0 & 0 & 0 & 0 & 0 & 0 & 0 & 0 & 0 & 0 & rs & st & 0 & 0 & 0 & 0 & 0 & 0 & rst & 0 & 0 & 0 & 0 \\
0 & 0 & t & 0 & 0 & 0 & 0 & 0 & 0 & 0 & 0 & 0 & 0 & 0 & 0 & 0 & 0 & 0 & 0 & rt & st & 0 & 0 & 0 & 0 & 0 & rst & 0 & 0 & 0 \\
0 & 0 & 0 & r & s & 0 & 0 & 0 & 0 & rt & st & 0 & 0 & 0 & 0 & 0 & 0 & 0 & 0 & 0 & 0 & rs & 0 & 0 & 0 & 0 & 0 & rst & 0 & 0 \\
0 & 0 & 0 & 0 & 0 & r & t & 0 & 0 & 0 & 0 & rs & st & 0 & 0 & 0 & 0 & 0 & 0 & 0 & 0 & 0 & rt & 0 & 0 & 0 & 0 & 0 & rst & 0 \\
0 & 0 & 0 & 0 & 0 & 0 & 0 & s & t & 0 & 0 & 0 & 0 & rs & rt & 0 & 0 & 0 & 0 & 0 & 0 & 0 & 0 & st & 0 & 0 & 0 & 0 & 0 & rst
\end{bmatrix}$$

03 EAS modes

Enhanced assumed strain

Enhanced strain field

$$\boldsymbol{\epsilon} = \boldsymbol{\epsilon}^{com} + \boldsymbol{\epsilon}^{EAS}$$

$$\boldsymbol{\epsilon}^{com} = \Delta^{s}\mathbf{u} = \mathbf{B}(r,s,t)\mathbf{U}$$

$$\boldsymbol{\epsilon}^{EAS} = \mathbf{G}(r,s,t)\boldsymbol{\alpha} = \frac{|\mathrm{J}_0|}{|J(r,s,t)|}\mathbf{F}_0^{-T}\mathbf{M}(r,s,t)\boldsymbol{\alpha}$$

$$[\mathbf{M}] = \left[\begin{array}{cccccccccccccccccccccccccccccc}
r & 0 & 0 & 0 & 0 & 0 & 0 & 0 & 0 & 0 & 0 & 0 & 0 & 0 & 0 & rs & rt & 0 & 0 & 0 & 0 & 0 & 0 & 0 & rst & 0 & 0 & 0 & 0 & 0 \\
0 & s & 0 & 0 & 0 & 0 & 0 & 0 & 0 & 0 & 0 & 0 & 0 & 0 & 0 & 0 & 0 & rs & st & 0 & 0 & 0 & 0 & 0 & 0 & rst & 0 & 0 & 0 & 0 \\
0 & 0 & t & 0 & 0 & 0 & 0 & 0 & 0 & 0 & 0 & 0 & 0 & 0 & 0 & 0 & 0 & 0 & 0 & rt & st & 0 & 0 & 0 & 0 & 0 & rst & 0 & 0 & 0 \\
0 & 0 & 0 & r & s & 0 & 0 & 0 & 0 & rt & st & 0 & 0 & 0 & 0 & 0 & 0 & 0 & 0 & 0 & 0 & rs & 0 & 0 & 0 & 0 & 0 & rst & 0 & 0 \\
0 & 0 & 0 & 0 & 0 & r & t & 0 & 0 & 0 & 0 & rs & st & 0 & 0 & 0 & 0 & 0 & 0 & 0 & 0 & 0 & rt & 0 & 0 & 0 & 0 & 0 & rst & 0 \\
0 & 0 & 0 & 0 & 0 & 0 & 0 & s & t & 0 & 0 & 0 & 0 & rs & rt & 0 & 0 & 0 & 0 & 0 & 0 & 0 & 0 & st & 0 & 0 & 0 & 0 & 0 & rst
\end{array}\right]$$

11 EAS modes

Enhanced assumed strain

Enhanced strain field

$$\boldsymbol{\epsilon} = \boldsymbol{\epsilon}^{com} + \boldsymbol{\epsilon}^{EAS}$$

$$\boldsymbol{\epsilon}^{com} = \Delta^s \mathbf{u} = \mathbf{B}(r, s, t)\mathbf{U}$$

$$\boldsymbol{\epsilon}^{EAS} = \mathbf{G}(r, s, t)\boldsymbol{\alpha} = \frac{|\mathrm{J}_0|}{|J(r, s, t)|}\mathbf{F}_0^{-T}\mathbf{M}(r, s, t)\boldsymbol{\alpha}$$

$$[\mathbf{M}] = \begin{bmatrix}
r & 0 & 0 & 0 & 0 & 0 & 0 & 0 & 0 & 0 & 0 & 0 & 0 & 0 & 0 & rs & rt & 0 & 0 & 0 & 0 & 0 & 0 & 0 & rst & 0 & 0 & 0 & 0 & 0 \\
0 & s & 0 & 0 & 0 & 0 & 0 & 0 & 0 & 0 & 0 & 0 & 0 & 0 & 0 & 0 & 0 & rs & st & 0 & 0 & 0 & 0 & 0 & 0 & rst & 0 & 0 & 0 & 0 \\
0 & 0 & t & 0 & 0 & 0 & 0 & 0 & 0 & 0 & 0 & 0 & 0 & 0 & 0 & 0 & 0 & 0 & 0 & rt & st & 0 & 0 & 0 & 0 & 0 & rst & 0 & 0 & 0 \\
0 & 0 & 0 & r & s & 0 & 0 & 0 & 0 & rt & st & 0 & 0 & 0 & 0 & 0 & 0 & 0 & 0 & 0 & 0 & rs & 0 & 0 & 0 & 0 & 0 & rst & 0 & 0 \\
0 & 0 & 0 & 0 & 0 & r & t & 0 & 0 & 0 & 0 & rs & st & 0 & 0 & 0 & 0 & 0 & 0 & 0 & 0 & 0 & rt & 0 & 0 & 0 & 0 & 0 & rst & 0 \\
0 & 0 & 0 & 0 & 0 & 0 & 0 & s & t & 0 & 0 & 0 & 0 & rs & rt & 0 & 0 & 0 & 0 & 0 & 0 & 0 & 0 & st & 0 & 0 & 0 & 0 & 0 & rst
\end{bmatrix}$$

24 EAS modes

Shape results

Numerical/experimental (DIC) comparison $Y = 0$

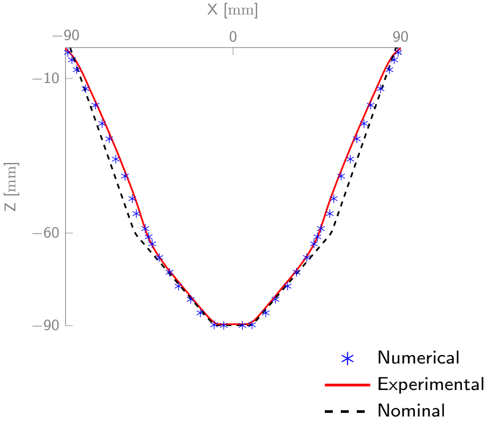

Shape results

Numerical/experimental (DIC) comparison $Y = 0$

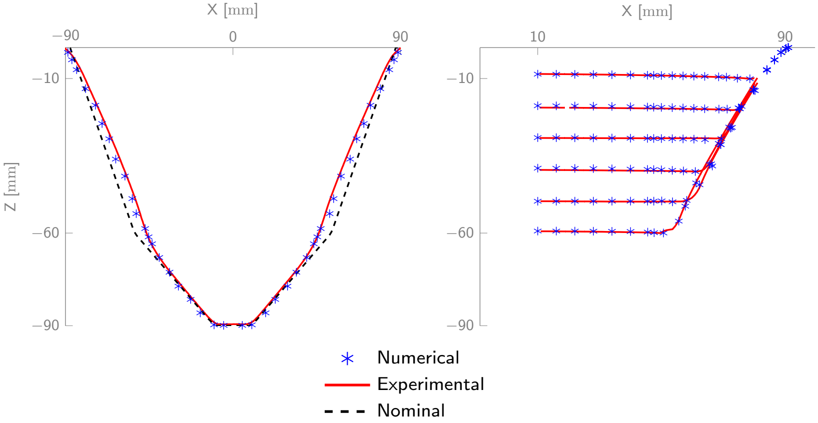

Shape results

Numerical/experimental (DIC) comparison $Y = 0$

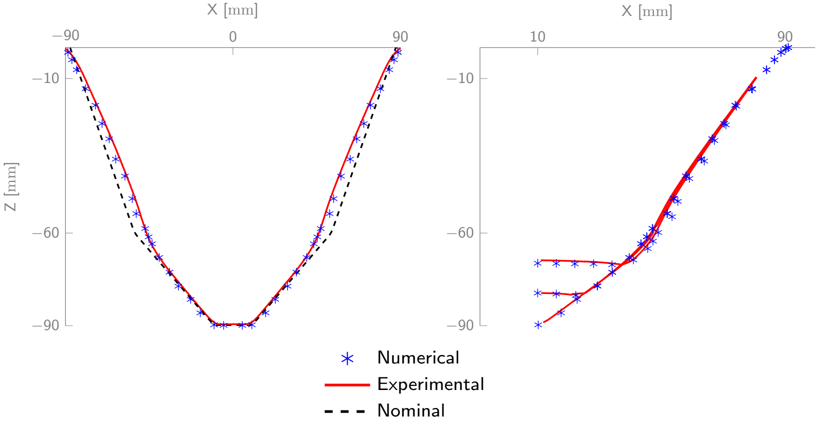

EAS and mesh influence

- Strong EAS mode influence.
- Small mesh influence.

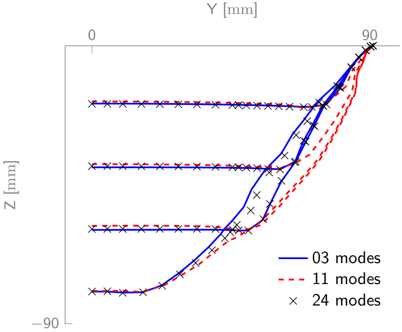

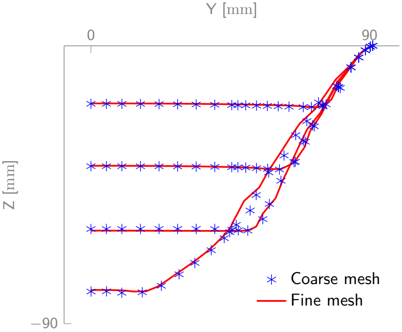

Force evolution

- Both EAS modes and mesh influence.

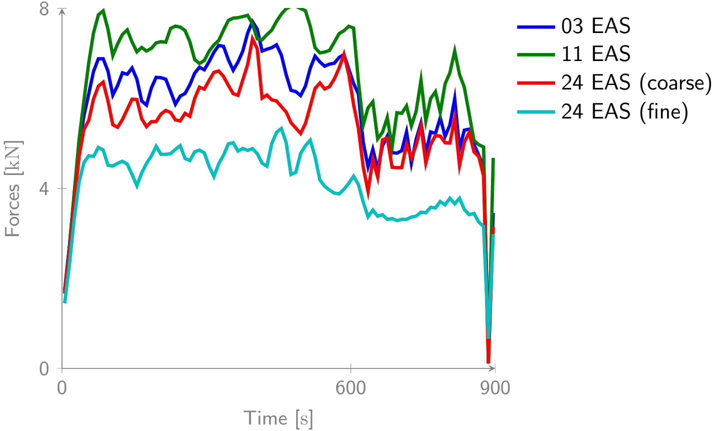

Contents

Ductile fracture

- The stress state has a strong influence on damage development and fracture.
- Triaxiality has been used to evaluate the stress state effect on damage/fracture.

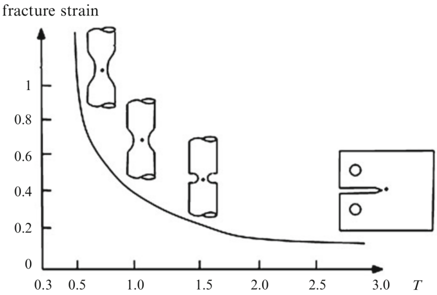

[Pineau and Pardoen, 2007]

Ductile fracture

- The stress state has a strong influence on damage development and fracture.
- Triaxiality has been used to evaluate the stress state effect on damage/fracture.

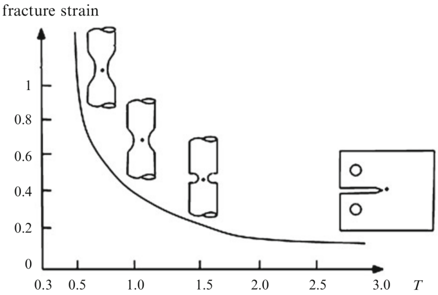

[Pineau and Pardoen, 2007]

$$T(I_1, J_2) = \frac{\sigma_m}{\sigma_{eq}} = \frac{1}{3\sqrt{3}} \frac{I_1}{\sqrt{J_2}}$$

- T ratio between volumetric I_1 and distorsion J_2 effects.
- $T \to 0 \Longrightarrow \epsilon_f \to \infty$

Ductile fracture

- Forming processes are characterized by low triaxialities.
- The failure mode (coalescence) is different at high/low triaxialities:

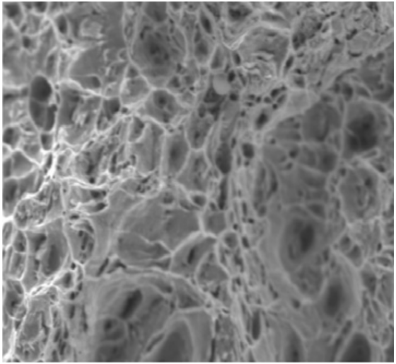

Cavity controlled (Dimples)
$T = 1.10$

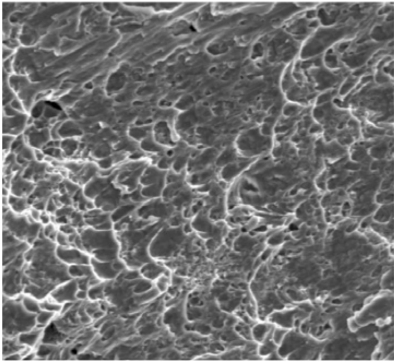

Shear controlled
$T = 0.47$

[Barsoum and Faleskog, 2007a]

Gurson model

- Given the Gurson [1977] model:

$$F = \frac{\sigma_{eq}^2}{\sigma_Y^2} - 1 + \underbrace{2f \cosh \frac{3}{2}\frac{\sigma_m}{\sigma_Y} - f^2}_{\text{Damage}} = 0$$

- No damage is predicted when $T = 0$. Further extensions are required.
- Gologanu et al. [1996] note that the void expansion can vary at same triaxialities.
- At low triaxiality, void shape evolution becomes more important than void growth.

Lode angle influence

- Triaxiality is not able to account the shape effects on voids.
- Solution: fully account the stress state with the set (I_1, J_2, J_3).
- A *physical meaning* can be asigned to J_3 through the **Lode angle** θ.

$$\begin{pmatrix} \sigma_1 \\ \sigma_2 \\ \sigma_3 \end{pmatrix} = \frac{I_1}{3} \begin{pmatrix} 1 \\ 1 \\ 1 \end{pmatrix} + \frac{2}{\sqrt{3}} \sqrt{J_2} \begin{pmatrix} \cos\theta \\ \cos(120 - \theta) \\ \cos(120 + \theta) \end{pmatrix}$$

- Stress state:
  - $\theta = 0$: uniaxial tension plus hydrostatic pressure (triaxial tension).
  - $\theta = 30$: pure shear plus hydrostatic pressure.
  - $\theta = 60$: uniaxial compression plus hydrostatic pressure.
- The relation between θ and J_3 is given by:

$$X(J_2, J_3) = \cos 3\theta = \frac{27}{2} \frac{J_3}{\sigma_{eq}^3}$$

Micromechanics

- Unit cell deformation at constant triaxiality $T = 1$.

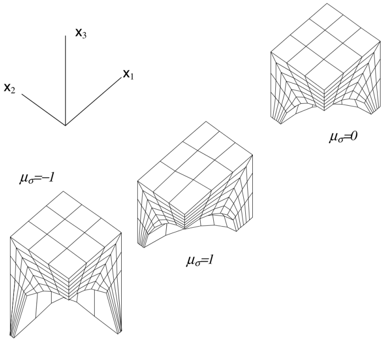

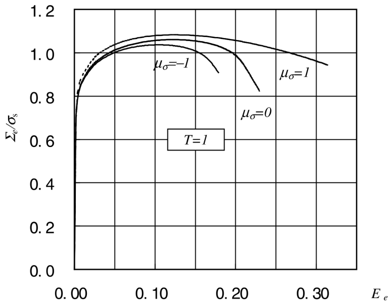

[Zhang et al., 2001]

Influence on fracture strain

- The strain at fracture is not monotonically decreasing function of the triaxiality.
- Note that the peaks are at different triaxialities.

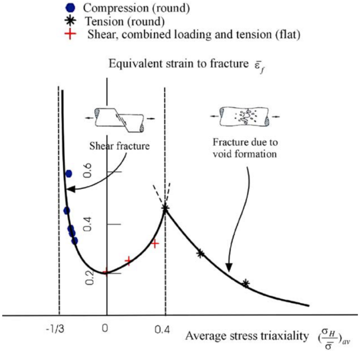

[Bao and Wierzbicki, 2004]

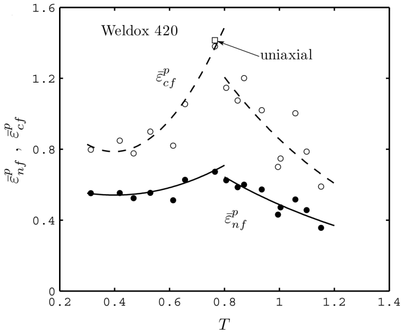

[Barsoum and Faleskog, 2007b]

Influence on fracture strain

- They are *lode angle independent* materials.

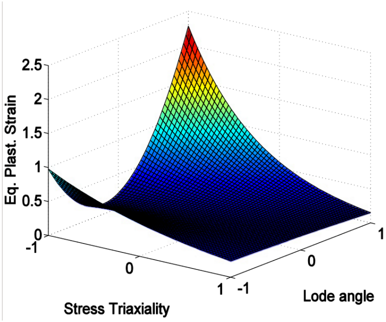

Aluminum 2024-T351

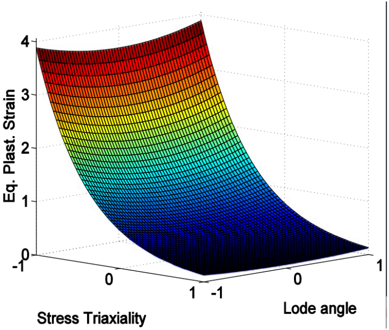

1045 steel

[Bai and Wierzbicki, 2008; Malcher et al., 2012]

Shear extension

Nahshon and Hutchinson [2008]

Void growth:

$$\dot{f} = \underbrace{(1-f)\mathrm{tr}\left(\dot{\boldsymbol{\epsilon}}^P\right)}_{\text{Classical}} + \underbrace{k_\omega f \omega(\mathbf{s}) \frac{\mathbf{s}\dot{\epsilon}^P}{\widehat{\sigma}_{eq}}}_{\text{Shear}}$$

(k_ω is a material constant)

Where:

$$\omega = 1 - \left(\frac{27}{2}\frac{J_3}{\sigma_{eq}}\right)^2 \qquad 0 \leq \omega \leq 1$$

Contents

Material parameters identification

- Characterization of a DC01 ferritic steel sheet (1 mm thickness).
- Test performed in the *Laboratoire de Mécanique des Matériaux et Structures*, ULg.

Classical tests

- Tensile test (RD, TD, 45°)
- Monotonic shear test (RD).
- Bauschinger shear test (RD).
- Plane strain tests (RD, TD, 45°).

Microphotographs
By Anne Mertens

- Void volume fraction measurements in the cracked specimens.

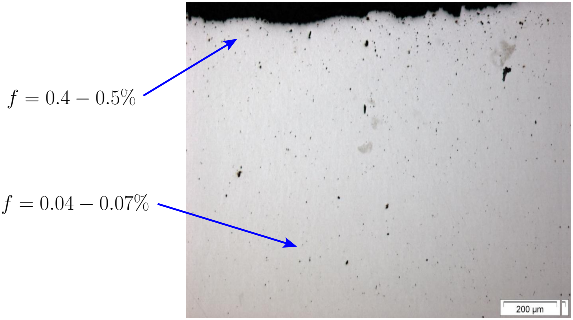

- Small void size, concentrated near the crack.
- For the shear tests, no voids growth is observed.

Microphotographs
By Anne Mertens

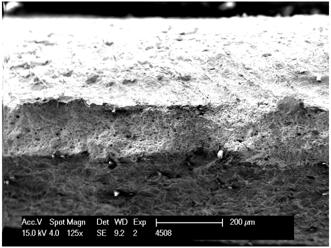

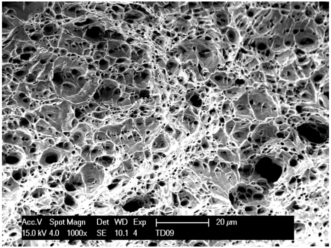

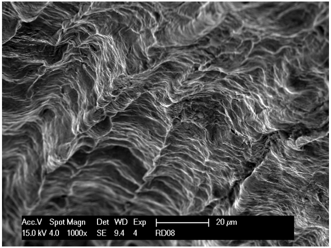

Contents

Current work

- **Numerical**: Gurson model extended to shear.
- **Experimental**: Test campaign to characterize Gurson.
- **Conference**: NUMISHEET14 article and benchmark.

Conferences and articles

Conferences articles

- **ESAFORM12**: Evaluation of the Enhanced Assumed Strain and Assumed Natural Strain in the SSH3D and RESS3 Solid Shell Elements
- **SheMet13**: Numerical simulation of a pyramid steel sheet formed by single point incremental forming using solid-shell finite elements.
- **ESAFORM13**: Towards fracture prediction in single point incremental forming.

Articles

- Study of the geometrical inaccuracy on a SPIF two-slope pyramid by finite element simulations. International Journal of Solids and Structures, 2011.

References I

Bai, Y., Wierzbicki, T., Jun. 2008. A new model of metal plasticity and fracture with pressure and Lode dependence. International Journal of Plasticity 24 (6), 1071–1096.

Bao, Y., Wierzbicki, T., Jan. 2004. On fracture locus in the equivalent strain and stress triaxiality space. International Journal of Mechanical Sciences 46 (1), 81–98.

Barsoum, I., Faleskog, J., Mar. 2007a. Rupture mechanisms in combined tension and shear-Experiments. International Journal of Solids and Structures 44 (6), 1768–1786.

Barsoum, I., Faleskog, J., Aug. 2007b. Rupture mechanisms in combined tension and shear-Micromechanics. International Journal of Solids and Structures 44 (17), 5481–5498.

Gao, X., Zhang, G., Roe, C., Jun. 2009. A Study on the Effect of the Stress State on Ductile Fracture. International Journal of Damage Mechanics 19 (1), 75–94.

Gologanu, M., Leblond, J.-B., Perrin, G., Devaux, J., 1996. Recent extensions of Gurson's model for porous ductile materials. International Seminar of Micromechanics, 61–130.

Gurson, A., 1977. Continuum theory of ductile rupture by void nucleation and growth: Part I-Yield criteria and flow rules for porous ductile media. Journal of Engineering Materials and Technology 99 (1), 2–15.

Henrard, C., Bouffioux, C., Eyckens, P., Sol, H., Duflou, J., van Houtte, P., Van Bael, A., Duchêne, L., Habraken, A. M., Dec. 2010. Forming forces in single point incremental forming: prediction by finite element simulations, validation and sensitivity. Computational Mechanics 47 (5), 573–590.

References II

Malcher, L., Andrade Pires, F., César de Sá, J., Mar. 2012. An assessment of isotropic constitutive models for ductile fracture under high and low stress triaxiality. International Journal of Plasticity 30-31, 81–115.

Nahshon, K., Hutchinson, J., Jan. 2008. Modification of the Gurson Model for shear failure. European Journal of Mechanics - A/Solids 27 (1), 1–17.

Pineau, A., Pardoen, T., 2007. Failure mechanisms of metals. Comprehensive structural integrity encyclopedia 2.

Zhang, K., Bai, J., François, D., Aug. 2001. Numerical analysis of the influence of the Lode parameter on void growth. International Journal of Solids and Structures 38 (32-33), 5847–5856.